nature physics
SUPPLEMENTARY INFORMATION
DOI: 10.1038/NPHYS2516

How basin stability complements the linear-stability paradigm

P. J. Menck, J. Heitzig, N. Marwan & J. Kurths

Here we present supplementary material that accompanies our paper *How Basin Stability Complements the Linear-Stability Paradigm*. The first section of the material contains a motivation of the conceptual model of Amazonian vegetation we use and a discussion of the mechanical damped driven pendulum. Both systems demonstrate that linear stability concepts are unreliable proxies of global stability. The second section contains details on our analysis of basin stability in synchronizing networks.

1 Linear Stability Fails at Indicating Global Stability

1.1 Conceptual Amazonian Vegetation Model

To motivate the simple growth equation that we use in the main text, we review the equilibrium model of Amazonian vegetation presented in ref. 5. Consider a region of the Amazon basin that is subdivided into cells having different dry season (d.s.) precipitation requirements for forest establishment. Assume that the frequency of cells whose d.s. precipitation requirement is p follows a normal distribution,

$$f(p) = \frac{1}{\sigma\sqrt{2\pi}}\, e^{-\frac{(p-\mu)^2}{2\sigma^2}}$$

with mean μ and standard deviation σ. Then the relative forest cover C in the region is related to the region's average d.s. precipitation P through

$$C(P) = \int_0^P f(p)dp. \tag{S1}$$

Forest cover increases overall precipitation because trees take up water stored in the soil and release it to the atmosphere via evapotranspiration. The total amount of d.s. precipitation in the region can therefore be expressed as

$$P(C) = P_{\text{in}} + C \cdot \Phi, \tag{S2}$$

where P_{in} is the precipitation inflow from other regions and Φ is the contribution of one unit of forest cover to overall precipitation. An arid region is characterized by low P_{in}.

Now imagine that the region has a certain level of forest cover C_{before} before global climatic climate change alters P_{in}. How will C change? A pictorial answer is given in Fig. S1.

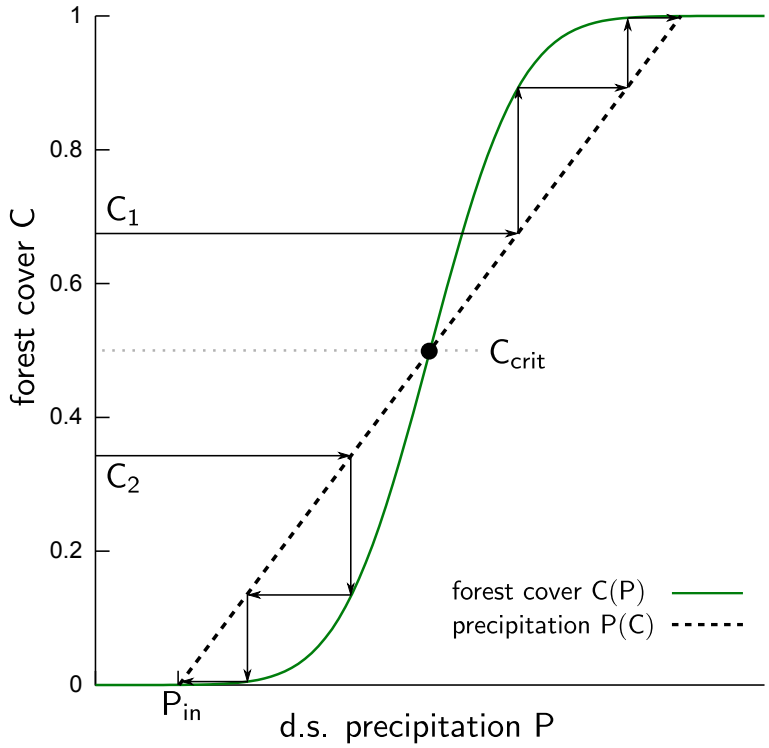

Supplementary Figure S1: **Equilibrium model of Amazonian vegetation.** The solid green line represents equilibrium forest cover C at d.s. precipitation P. The dashed black line is the overall d.s. precipitation P as a function of C. Step-stair sequences are shown for two different initial values of forest cover. Reproduced from ref. 5.

The solid green line represents equilibrium forest cover C at d.s. precipitation P, cf. eq. (S1). The dashed black line is the overall d.s. precipitation P at forest cover C, cf. eq. (S2). If $C_{\mathrm{before}} = C_1$, forest cover is above the critical threshold C_{crit}, so that P can support even more trees. Hence C grows, therefore P increases, upon which C grows further, and so on. Finally, due to this positive feedback loop, C is propelled towards 1.0. If, on the contrary, $C_{\mathrm{before}} = C_2$, forest cover is below C_{crit}. Forest cover at this level cannot be supported by P, starts to die back, again triggers a positive feedback loop, and eventually vanishes completely.

We describe the growth dynamics using the Levins model[31], a widely accepted basic vegetation model[32], to which we add a non-smooth switch in the growth term (corresponding to the limit $\sigma \ll \Phi$):

$$\frac{\mathrm{d}C}{\mathrm{d}t} = F(C) = \begin{cases} r(1-C)\,C - x\,C & \text{if} \quad C > C_{\mathrm{crit}}, \\ -x\,C & \text{if} \quad C < C_{\mathrm{crit}}. \end{cases}$$

According to this model, forest cover C grows with the saturating rate r if $C > C_{\mathrm{crit}}$ and dies with rate x (assuming $r > x > 0$). This model has two equilibria, the forest state $C_{\mathrm{F}} = 1 - \frac{x}{r}$ and the savanna state $C_{\mathrm{S}} = 0$. The equilibrium C_{F} (resp. C_{S}) exists and is stable if $C_{\mathrm{F}} > C_{\mathrm{crit}}$ (resp. $C_{\mathrm{crit}} > 0$). So, as in the equilibrium model reviewed above, C converges to a non-zero constant value if $C > C_{\mathrm{crit}}$ and vanishes completely otherwise. When increasing aridity drives up C_{crit}: i) C_{F}'s basin of attraction of shrinks, implying that C_{F} becomes less stable against perturbations such as strong deforestation (cf. Fig. 2). ii) C_{F} vanishes at $C_{\mathrm{crit}} = C_{\mathrm{F}}$.

Our model is conceptual. We do not intend it to serve as a description of reality. Rather, we use it as a reality-inspired aide to theory to illustrate the difference between the realm of small perturbations and the realm of non-small perturbations. This difference manifests itself in two phenomena:

i) As the linear stability coefficient of the forest state, $F'(C_{\mathrm{F}}) = x - r$, is a constant independent of C_{crit}, critical slowing down does not take place. This is reflected by a zero recovery exponent[33]. Indeed, critical slowing down may be absent in systems in which strong non-linearities such as switches exist.

ii) More important to us, because of their local nature, linear stability and the small-perturbation convergence rate do not sense that C_{F}'s basin of attraction of shrinks as C_{crit} goes up. The authors of ref. 34 write that "transitions caused by a sudden large disturbance without a preceding gradual loss of [stability against non-small perturbations][a] will not be announced by slowing down." On top of that, our model shows that slowing down may be absent *even if* such a gradual loss of stability is going on.

We conclude from this that linear stability and the small-perturbation convergence rate are *unreliable proxies* of how stable a state is against non-small perturbations. Instead of employing such local proxies, one should study global stability concepts like the one we suggest: basin stability.

The same conclusions can be drawn from the study of a basic damped driven pendulum (see next subsection).

[a]The original term they use is "resilience", refering to Holling's concept discussed in the main text.

1.2 Damped Driven Pendulum

Consider a classical damped pendulum driven by a constant angular acceleration T. Assume its dynamics to obey

$$\begin{aligned} \dot{\phi} &= \omega \\ \dot{\omega} &= -\alpha\omega + T - K\sin\phi, \end{aligned}$$

where $\alpha > 0$ is the dissipation coefficient and $K = g/\ell$, with the gravitational acceleration g and the pendulum's length ℓ.

In the following, we investigate the pendulum's solution space by varying $T \geq 0$ at fixed K, α ($T \leq 0$ reveals the mirror image). For $0 \leq T \leq K$, the pendulum has two fixed points $\mathbf{x}_i = (\phi_i, \omega_i)$, $i = 1, 2$, with coordinates

$$\begin{aligned} \phi_{1,2} &= \arcsin\left(\frac{T}{K}\right), \\ \omega_{1,2} &= 0 \end{aligned}$$

where we take ϕ_1 to be the solution of arcsin inside $[0, \pi/2]$ and $\phi_2 = \pi - \phi_1$. The eigenvalues of the Jacobian matrix at (ϕ_i, ω_i) read

$$\xi_i^{\pm} = -\frac{\alpha}{2} \pm \frac{\sqrt{\alpha^2 - 4K\cos\phi_i}}{2} \tag{S3}$$

and the maximum Lyapunov exponent of fixed point i is $\lambda_i = \mathrm{Re}\,\xi_i^{+}$. For $0 < T < K$, $\lambda_1 < 0$ and $\lambda_2 > 0$, because $\cos\phi_1 = -\cos\phi_2 > 0$. Hence the first fixed point $\mathbf{x}_1$ is a stable equilibrium and the second fixed point $\mathbf{x}_2$ is an unstable saddle. At $T = K$, a fold bifurcation occurs in which the two fixed points collide and disappear.

For $T > K$, the angular acceleration due to gravity cannot balance T and the pendu-

lum converges to a stable limit cycle in which ω oscillates around T/α. This limit cycle is also stable for a certain range $T_{\text{mult}} \leq T \leq K$. For these values of T, the pendulum is *multistable*. An example multistable state space is depicted in Supplementary Fig. S2.

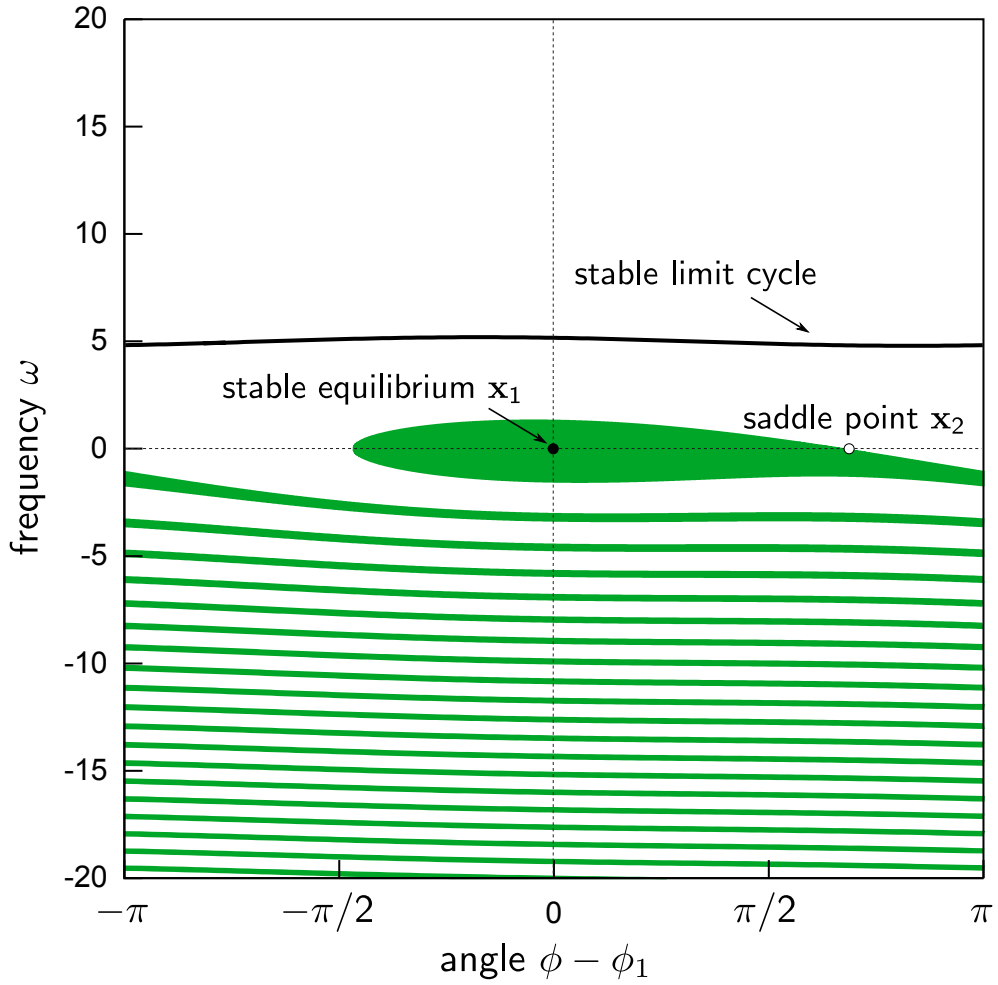

Supplementary Figure S2: **Phase Space of the Damped Driven Pendulum.** The filled (open) circle marks the stable equilibrium point $\mathbf{x}_1$ (the unstable saddle point $\mathbf{x}_2$). $\mathbf{x}_1$'s basin of attraction is indicated by the green area. From points in the non-coloured area, the pendulum converges to the limit cycle. We use $\alpha = 0.1$, $K = 1$, and $T = 0.5$.

For concreteness, we now choose $\alpha = 0.1$ and $K = 1$ and increase T from 0. First we look at linear stability. Supplementary Fig. S3 shows how the maximum Lyapunov

exponent λ_1 of the stable equilibrium $\mathbf{x}_1$ depends on T: Except very close to $T = 1$, λ_1 is *constant* and equal to $-\alpha/2$. Only at $T = 0.999997$, when the square root term contributing to the eigenvalues $\xi_1^{\pm}$ becomes real, does λ_1 start moving towards 0, where it reaches at $T = 1$.

Is critical slowing down, i.e., the decline of the small-perturbation convergence rate before the bifurcation, detectable *experimentally*? The maximum perturbation in positive ϕ-direction that the stable equilibrium $\mathbf{x}_1$ can withstand is $\phi_2 - \phi_1$ (cf. Supplementary Fig. S2), which at $T = 0.999997$ amounts to approximately $5 \cdot 10^{-3}$ rad $= 0.28°$. For a pendulum of length $\ell = 10$ cm, this corresponds to a displacement $\Delta = 0.5$ mm. Therefore, only if fluctuations induced by the environment are significantly less than Δ will critical slowing down be detectable in an experiment.

If critical slowing down is detectable, it occurs *very late* as T increases from 0 to 1. Hence critical slowing down appears not to be a reliable *early*-warning signal for the pendulum's critical transition.

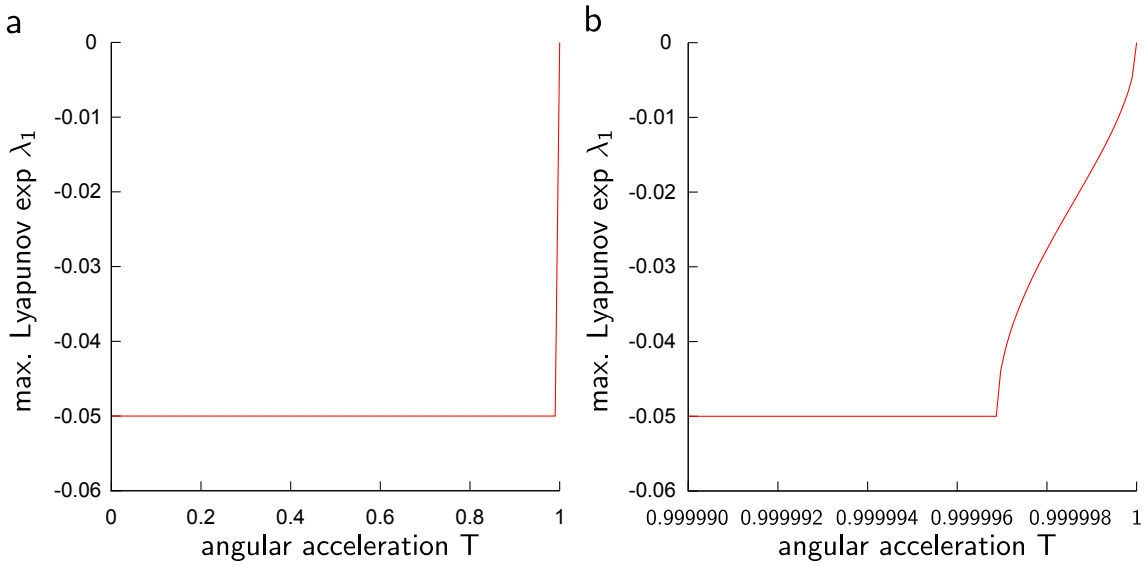

Supplementary Figure S3: **Linear Stability of the Damped Driven Pendulum. a,b:** Max. Lyapunov exp. λ_1 of the stable equilibrium versus T. **b** zooms in close to $T = 1$. We use $\alpha = 0.1$, $K = 1$.

Now we look at basin stability. To estimate $\mathbf{x}_1$'s basin stability $S_{\mathcal{B}}$, we randomly draw 1000 initial conditions from $[0, 2\pi] \times [-20, 20]$, integrate the system equations, and count in how many cases $\mathbf{x}_1$ (instead of the stable limit cycle) is reached. The result is shown in Supplementary Fig. S4. The limit cycle becomes stable at $T_{\text{mult}} \approx 0.13$. For $T \in [T_{\text{mult}}, 1)$, the pendulum is multistable. As T increases in this interval, basin stability $S_{\mathcal{B}}$ declines rapidly towards zero, where it reaches at $T = 1$.

None of this is indicated by the maximum Lyapunov exponent (cf. Supplementary Fig. S3a). Hence linear stability seems not to be a good proxy for the degree of stability against non-small perturbations.

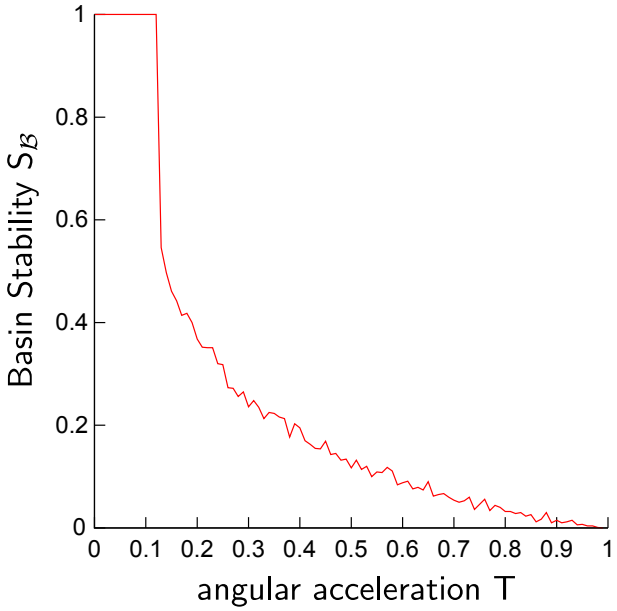

Supplementary Figure S4: **Basin Stability of the Damped Driven Pendulum.** Basin stability $S_{\mathcal{B}}$ of the stable equilibrium $\mathbf{x}_1$ versus T. We use $\alpha = 0.1$, $K = 1$.

2 Basin Stability in Synchronizing Networks

This section is ordered as follows. In the first subsection, we review the seminal study[11] by *Pecora and Carroll* on networks of identical oscillators that proposed the *Master Stability Function* (MSF) formalism and motivated the definition of *synchronizability*. In the second subsection, we elaborate on the computation of basin stability in Rössler networks. In the third subsection, we report properties of the real-world networks referred to in Fig. 4. The fourth subsection contains remarks about the non-convexity of the synchronous state's basin of attraction in Rössler networks.

2.1 Master Stability Function Formalism

Consider a system of N identical oscillators which are coupled through a connected network. Its dynamics are governed by the equations

$$\dot{\mathbf{r}}_i = \mathbf{F}(\mathbf{r}_i) + K \sum_j A_{ij}[\mathbf{H}(\mathbf{r}_j) - \mathbf{H}(\mathbf{r}_i)] = \mathbf{F}(\mathbf{r}_i) - K \sum_j L_{ij}\mathbf{H}(\mathbf{r}_j),$$

where $\mathbf{r}_i$ is the m-dimensional state vector describing the processes at node i. A is the adjacency matrix, with $A_{ij} = 1$ if there is an edge between nodes i and j and $A_{ij} = 0$ otherwise. $L_{ij} = \delta_{ij} \sum_k A_{ik} - A_{ij}$ is the Laplacian matrix with $\delta_{ij} = 1$ if $i = j$ and $\delta_{ij} = 0$ otherwise. Finally, K denotes the overall coupling constant and $\mathbf{H}(\mathbf{r})$ is the coupling function prescribing through which of their m components the connected nodes interact. $\mathbf{F}$ determines the evolution of each individual oscillator in the case of no coupling ($K = 0$). Because L_{ij} has zero row sum by definition, there always exists a synchronous state $\mathcal{M}_s = \{\mathbf{r}_1 = \mathbf{r}_2 = \ldots = \mathbf{r}_N = \mathbf{s}(t) | t \in \mathbb{R}\}$ in the Nm-dimensional state space in which all individual oscillators follow the same trajectory $\mathbf{s}(t)$. Technically, $\mathcal{M}_s$ is an invariant set of states rather than a state. However, for notational simplicity, we keep on calling it *the synchronous state.*

Is $\mathcal{M}_s$ stable? Based on linear stability, this problem was elegantly shown[11] to break up into two parts: Firstly, $\mathbf{F}, \mathbf{H}$ define a Master Stability Function $\mathrm{MSF}_{\mathbf{F},\mathbf{H}}$ that is independent of the network. Secondly, K and the network define a set of numbers at which $\mathrm{MSF}_{\mathbf{F},\mathbf{H}}$ has to be evaluated to find out whether $\mathcal{M}_s$ is stable. Indeed, $\mathcal{M}_s$ is stable if K and the eigenvalues $\lambda_1 = 0 < \lambda_2 \leq \ldots \leq \lambda_N$ of the positive semidefinite symmetric matrix L satisfy $\mathrm{MSF}_{\mathbf{F},\mathbf{H}}(K\lambda_i) < 0$ for all $i = 2, \ldots, N$. This condition is equivalent to demanding that all transverse eigenmodes of $\mathcal{M}_s$ have a negative Lyapunov exponent. Many choices of $\mathbf{F}$ and $\mathbf{H}$ yield a function $\mathrm{MSF}_{\mathbf{F},\mathbf{H}}$ that is negative only in an interval (α_1, α_2), so that $\mathcal{M}_s$ is stable if $\alpha_1 < K\lambda_i < \alpha_2$ for all $i = 2, \ldots, N$. This can only be fulfilled if $\lambda_N/\lambda_2 < \alpha_2/\alpha_1$, in which case the synchronous state is stable, provided K is chosen from the *stability interval* $I_s = (\alpha_1/\lambda_2, \alpha_2/\lambda_N)$. In the main text, $\lambda_2 =: \lambda_{\min}$, $\lambda_N =: \lambda_{\max}$, and $\beta = \alpha_2/\alpha_1$ is referred to as the *stability threshold*. Note that $\lambda_2 > 0$ if the network is connected as we have assumed here.

2.2 Basin Stability in Rössler networks

We study ensembles of Watts-Strogatz (WS) networks consisting of N Rössler oscillators that are coupled through their x-components. In each network, the dynamics of the oscillator at node i is determined by the equations

$$\begin{aligned} \dot{x}_i &= -y_i - z_i - K\sum_{j=1}^{N} L_{ij}x_j \\ \dot{y}_i &= x_i + ay_i \\ \dot{z}_i &= b + z_i(x_i - c) \end{aligned}$$

with $a = b = 0.2$ and $c = 7.0$. L is the network's Laplacian matrix and K is the overall coupling constant. We are interested in the stability of the synchronous state in which all oscillators follow the same trajectory on the Rössler attractor. According to the Master Stability Function formalism (see previous subsection), this state is stable if the network's synchronizability $R = \lambda_{\max}/\lambda_{\min}$ is lower than the threshold α_2/α_1, provided the coupling K is selected from the stability interval $I_s := (\alpha_1/\lambda_{\min}, \alpha_2/\lambda_{\max})$ (for x-coupled Rössler oscillators, $\alpha_1 = 0.1232$ and $\alpha_2 = 4.663$).

Fig. 3a displays that for ensemble networks with too small WS rewiring probability p the expected synchronizability $\langle R\rangle$ has not yet crossed α_2/α_1 so that the synchronous state is not stable (note the reversed y-axis in the Figure). But the expected synchronizability improves rapidly, soon passes the stability threshold, and then improves even further. However, the level of synchronizability just qualifies the synchronous state as stable or unstable. To quantify stability, we label by $S_{\mathcal{B}}$ the basin stability of the synchronous state. Being a relative measure of the basin's volume (see Methods), $S_{\mathcal{B}}$ is a number between 0 and 1. For each ensemble network we compute the mean basin stability $\bar{S}_{\mathcal{B}}$ by averaging over $S_{\mathcal{B}}(K)$ for several values of K within the stability interval. Strikingly, Figure 3b reveals that the expected mean basin stability $\langle\bar{S}_{\mathcal{B}}\rangle$ shows a behaviour opposite to that of

the expected synchronizability: After shooting up initially, expected mean basin stability $\langle \bar{S}_{\mathcal{B}} \rangle$ declines exponentially fast as the rewiring probability p increases. (This true for all choices of N and k that we analyzed, see Supplementary Fig.S5).

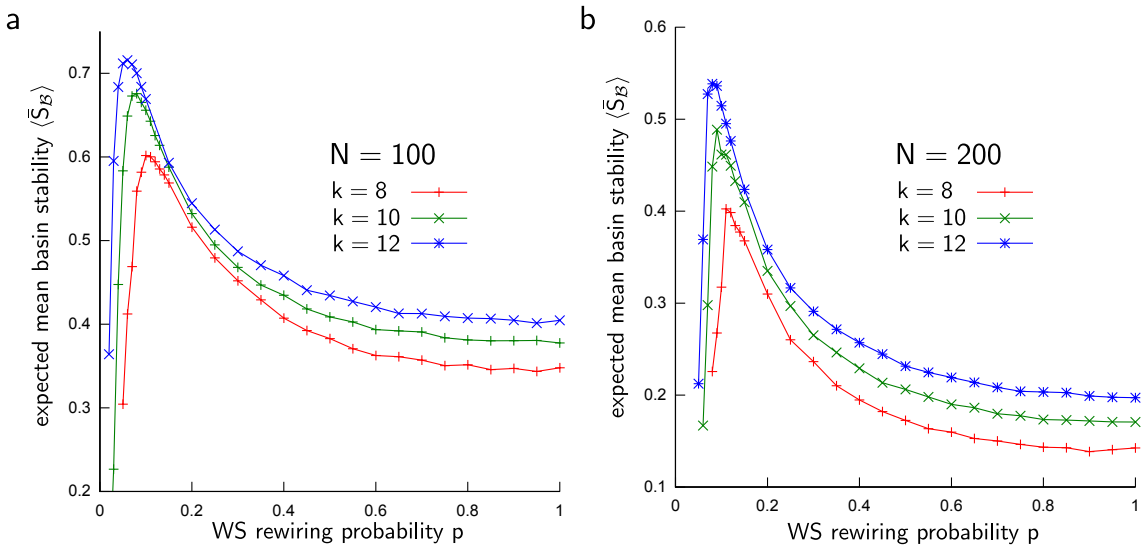

Supplementary Figure S5: **Basin Stability in Rössler networks.** Expected basin stability $\langle \bar{S}_{\mathcal{B}} \rangle$ versus p. Solid lines are guides to the eye. **a**: $N = 100$, **b**: N=200.

2.2.1 Qualitative Explanation

Why is this? Supplementary Fig. S6a displays that the expected basin stability $\langle S_{\mathcal{B}}(K)\rangle$ of a network at any fixed coupling K increases strongly as K grows and that it hardly depends on p. Hence a network's mean basin stability $\bar{S}_{\mathcal{B}}$ should be determined primarily by the location of its stability interval I_s. Indeed, for increasing p the expected stability interval $\langle I_s\rangle$ of a network significantly shifts to the left and simultaneously broadens (see Supplementary Fig. S6b). This qualitatively explains the rapidly decreasing behaviour of the expected mean basin stability shown in Fig. 3b. It also implies that the mean basin stability $\bar{S}_{\mathcal{B}}$ of a Rössler network mainly depends on the absolute values of $\lambda_{\min}$ and $\lambda_{\max}$ (which determine I_s), as opposed to their ratio which is central in synchronizability studies.

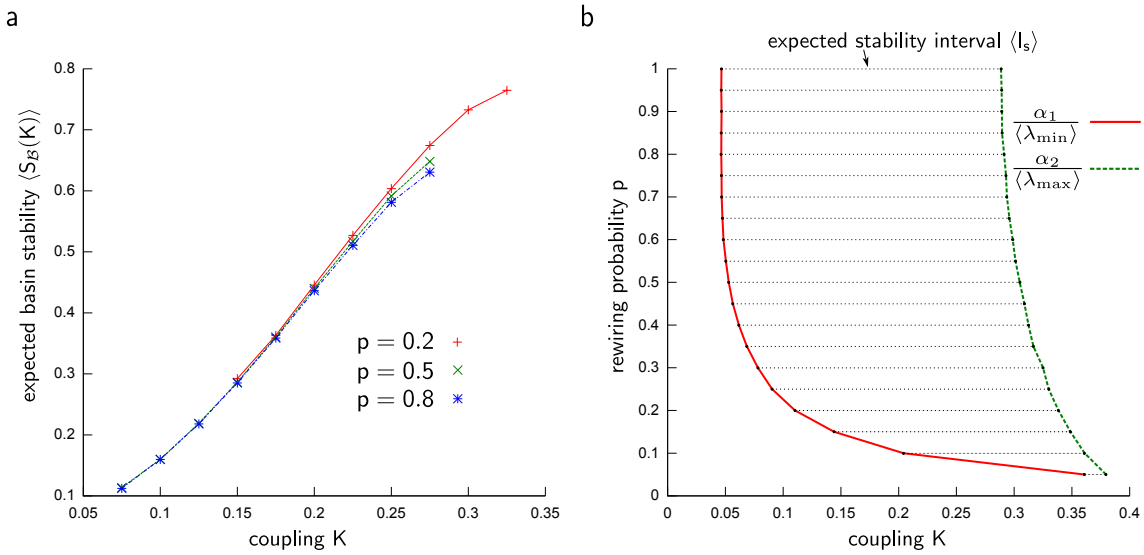

Supplementary Figure S6: **Explanatory characteristics.** **a**: expected basin stability $\langle S_{\mathcal{B}}(K)\rangle$ at coupling K, measured in the interior of the expected stability interval for $p = 0.2, 0.5, 0.8$. Solid lines are guides to the eye. **b**: expected stability interval $\langle I_s\rangle$ at rewiring probability p. The red solid line represents its left bound $\alpha_1/\langle\lambda_{\min}\rangle$, the green dashed line its right bound $\alpha_2/\langle\lambda_{\max}\rangle$.

2.2.2 Example Estimation of Mean Basin Stability $\bar{S}_{\mathcal{B}}$

For the sake of reproducibility, here we report the estimation of mean basin stability $\bar{S}_{\mathcal{B}}$ for an example network from the ensemble. Its edge list reads:

0-1	0-2	0-3	4-61	2-91	1-3	1-4	1-5	3-20	2-4	2-5	2-6	3-4	3-5	3-6	3-7
4-5	4-6	7-73	4-8	5-6	5-7	5-8	5-9	7-88	8-45	6-9	6-10	7-8	7-9	7-10	7-11
8-9	8-10	8-11	8-12	9-10	9-11	9-12	9-13	10-11	10-12	10-13	10-14	12-93	11-13	14-3	11-15
12-13	12-14	12-15	12-16	14-49	13-15	13-16	13-17	14-15	14-16	14-17	14-18	15-16	15-17	15-18	19-65
16-17	16-18	16-19	20-94	17-18	17-19	17-20	17-21	18-19	20-65	18-21	18-22	19-20	19-21	19-22	19-23
20-21	22-16	20-23	20-24	21-22	21-23	24-0	21-25	22-23	22-24	22-25	22-26	24-47	23-25	23-26	27-75
24-25	26-34	27-17	28-90	25-26	25-27	28-8	25-29	26-27	26-28	26-29	26-30	27-28	27-29	27-30	27-31
28-29	30-46	31-36	28-32	30-70	29-31	29-32	29-33	30-31	30-32	30-33	30-34	31-32	31-33	31-34	35-52
32-33	32-34	35-6	36-48	33-34	33-35	33-36	33-37	34-35	34-36	34-37	34-38	35-36	35-37	35-38	35-39
36-37	36-38	39-73	36-40	37-38	37-39	40-84	37-41	38-39	38-40	38-41	42-93	39-40	41-46	39-42	43-13
40-41	40-42	43-86	40-44	41-42	41-43	41-44	45-67	42-43	42-44	45-77	46-95	43-44	43-45	43-46	43-47
44-45	44-46	44-47	44-48	45-46	47-60	45-48	49-75	46-47	46-48	46-49	46-50	47-48	47-49	47-50	51-96
48-49	48-50	48-51	52-34	49-50	49-51	49-52	49-53	50-51	50-52	50-53	50-54	51-52	51-53	51-54	51-55
53-28	54-21	52-55	56-83	54-1	53-55	56-88	57-88	55-79	54-56	54-57	58-78	56-85	55-57	55-58	55-59
56-57	56-58	56-59	56-60	57-58	57-59	60-45	57-61	58-59	58-60	61-36	62-75	60-71	59-61	59-62	63-12
61-33	60-62	60-63	64-7	61-62	61-63	61-64	61-65	62-63	62-64	62-65	66-77	63-64	63-65	66-74	67-47
64-65	64-66	67-95	68-19	65-66	65-67	65-68	65-69	66-67	66-68	66-69	66-70	67-68	67-69	67-70	67-71
68-69	68-70	68-71	68-72	69-70	69-71	69-72	73-14	70-71	70-72	73-18	74-16	71-72	71-73	71-74	71-75
72-73	72-74	72-75	72-76	74-47	73-75	73-76	77-56	75-10	74-76	74-77	74-78	75-76	75-77	75-78	75-79
77-10	76-78	79-97	76-80	77-78	77-79	77-80	77-81	78-79	78-80	81-93	78-82	79-80	79-81	79-82	79-83
80-81	80-82	83-30	80-84	81-82	81-83	84-14	81-85	82-83	82-84	82-85	86-52	84-50	83-85	83-86	83-87
85-51	86-72	84-87	84-88	85-86	85-87	85-88	85-89	86-87	86-88	86-89	86-90	87-88	87-89	87-90	91-12
88-89	88-90	88-91	88-92	90-97	91-25	89-92	89-93	91-10	92-65	90-93	90-94	92-54	91-93	94-15	91-95
92-93	92-94	92-95	92-96	93-94	93-95	93-96	93-97	95-18	94-96	94-97	94-98	95-96	95-97	95-98	99-59
96-97	96-98	96-99	0-34	98-60	97-99	97-0	97-1	98-99	98-0	98-1	98-2	99-0	99-1	99-2	99-3

This network consists of $N = 100$ nodes and $E = 400$ edges (and was generated using the Watts-Strogatz model with rewiring probability $p = 0.2$). The minimum and maximum non-zero eigenvalues of its Laplacian matrix are $\lambda_{\min} = 1.236$ and $\lambda_{\max} = 13.87125$, respectively. Hence its stability interval $I_s = (0.010, 0.336)$. The synchronous state is stable for $K \in I_s$. We measure its basin stability at 11 different equally spaced values of K in the interior of I_s, namely 0.119, 0.139, 0.159, 0.179, 0.198, 0.218, 0.238, 0.258, 0.278, 0.297, 0.317, and obtain the corresponding sequence of $S_{\mathcal{B}}$-values: 0.226, 0.274, 0.330, 0.346, 0.472, 0.496, 0.594, 0.628, 0.656, 0.694, 0.690. To estimate the mean basin stability $\bar{S}_{\mathcal{B}}$ of this network, we compute the average of these values and obtain $\bar{S}_{\mathcal{B}} \approx 0.49$.

2.2.3 2-dimensional Watts-Strogatz Networks

In the main text and in the preceding sections of this supplementary material, we use a 1-dimensional ring as the initial configuration of the Watts-Strogatz algorithm. Here, we use the 2-dimensional lattice depicted in Supplementary Fig. S7.

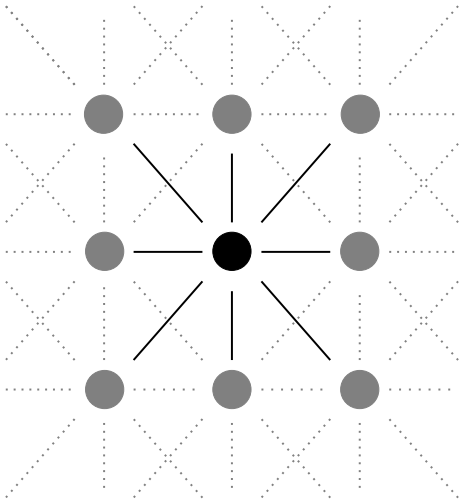

Figure S7: **Initial grid for 2-dimensional Watts-Strogatz (WS) network generation.** Each node is connected to its four nearest neighbours and the four diagonal ones among its next-nearest neighbours. So each node has 8 links.

We choose $N = 20 \cdot 20 = 400$ as the network size and, as before, place a Rössler oscillator at each node. Note that basin stability calculations on this lattice size approach the limits of what is computationally feasible today. For each network in the ensemble we estimate the basin stability $S_{\mathcal{B}}(K)$ for several $K \in I_s$ and compute their mean $\bar{S}_{\mathcal{B}}$. Here, we use a slightly smaller reference subset, $\mathcal{Q} = q^N$ with $q = [-15, 15] \times [-15, 15] \times [-4, 35]$, than above as otherwise the values of $S_{\mathcal{B}}$ are too small to be accuractely measurable with $T = 500$ integrations (cf. Methods). Note that the Rössler attractor is still included in q. Finally, we average $\bar{S}_{\mathcal{B}}$ over the ensemble to obtain $\langle \bar{S}_{\mathcal{B}} \rangle$.

The results are shown in Supplementary Fig. S8. There is no qualitative difference to Fig. 3: Whereas synchronizability improves as networks become more random, expected

basin stability is larger in networks that are more regular and falls off exponentially with increasing randomness.

Supplementary Fig. S9 shows how the 2-dimensional results compare topologically to synchronizing networks from the real-world (cf. Fig. 4). Again, there is no qualitative difference. Whereas the need for good synchronizability drives networks towards randomness, the need for large basin stability drives them towards regularity.

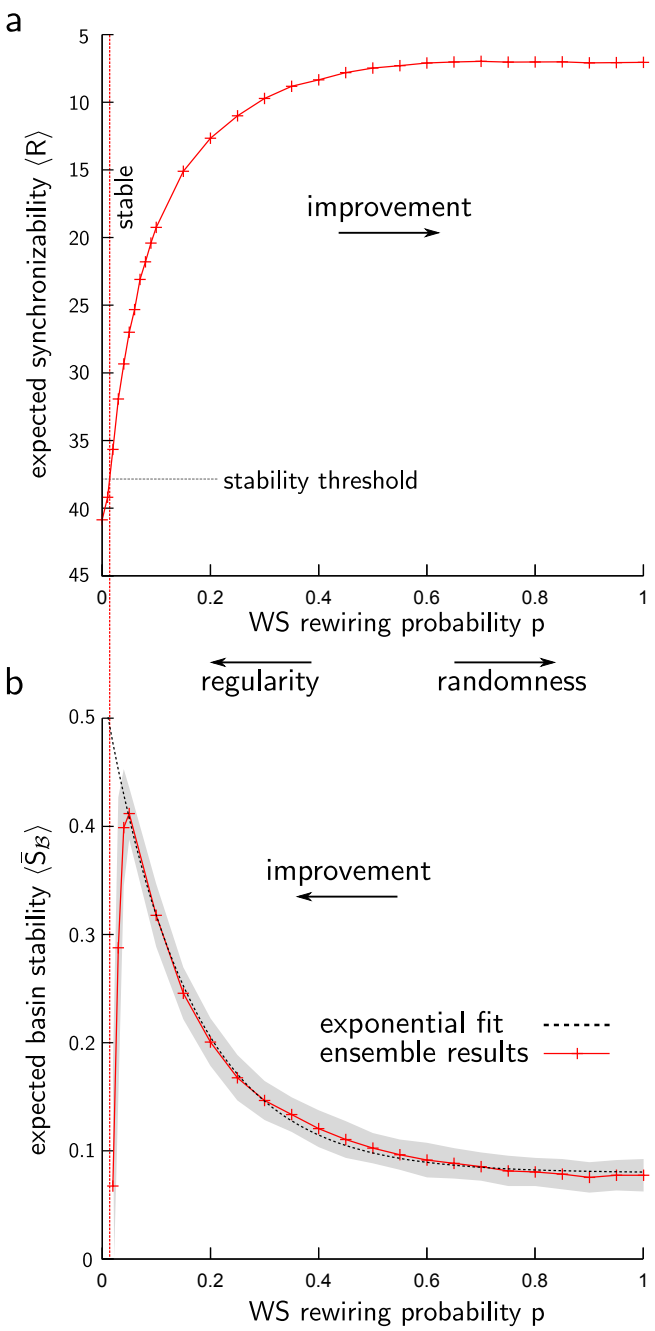

Figure S8: **Synchronizability and basin stability in 2-dimensional Watts-Strogatz (WS) networks of chaotic oscillators.** **a**: Expected synchronizability $\langle R \rangle$ versus the WS model's parameter p. The scale of the y-axis was reversed to indicate improvement upon increase in p. **b**: Expected basin stability $\langle \bar{S}_{\mathcal{B}} \rangle$ versus p. The grey shade indicates $\pm$ one standard deviation. The dashed line shows an exponential fitted to the ensemble results for $p \geq 0.05$. Solid lines are guides to the eye. The plots shown were obtained for $N = 400$ oscillators of Rössler type, each having on average $k = 8$ neighbours.

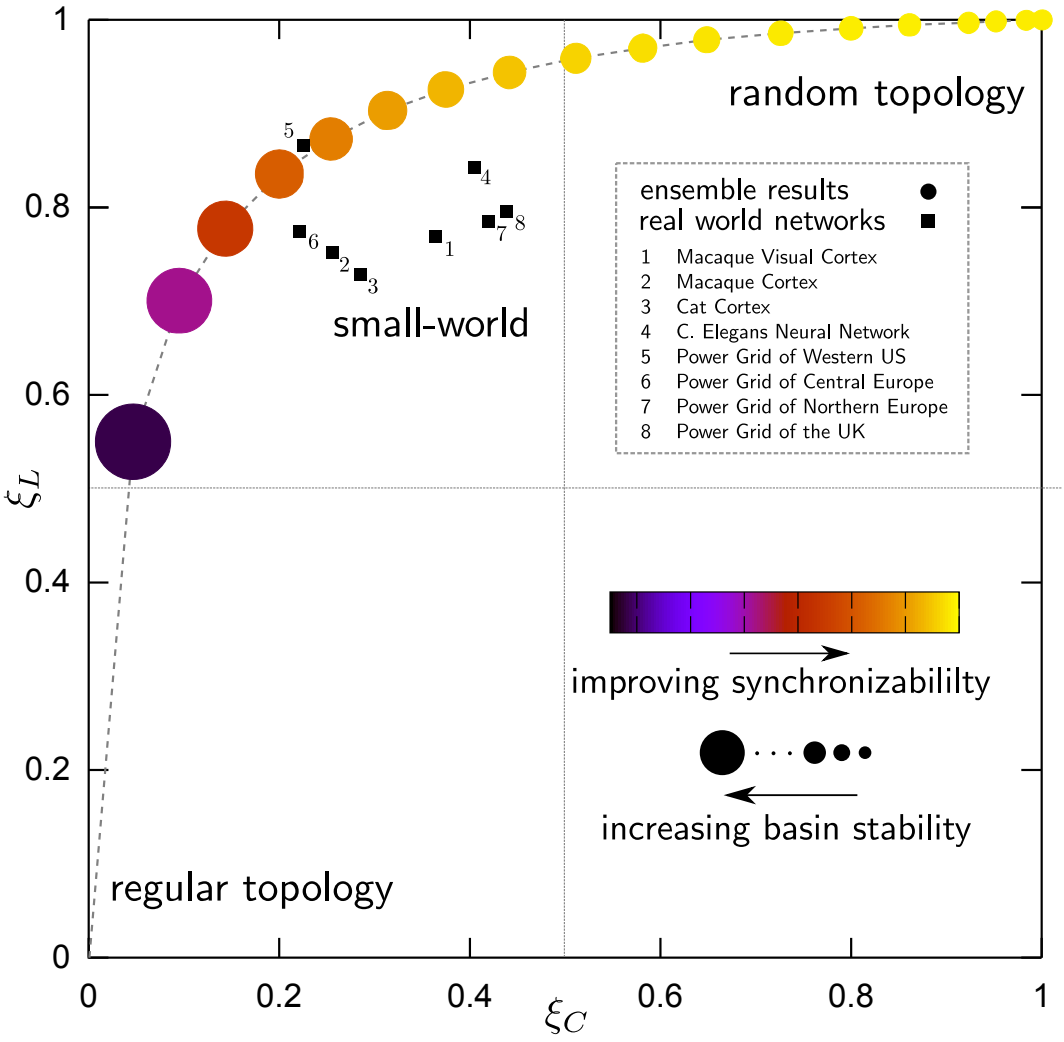

Figure S9: **Topological comparison of results for the 2-dimensional ensemble with real-world networks.** A circle represents the results for 2D Watts-Strogatz networks with $N = 400$, $k = 8$ and rewiring probability $p \in \{0.05, 0.1, 0.15, \ldots, 1.0\}$ (p increasing from left to right). A circle's area is proportional to the expected basin stability $\langle \bar{S}_{\mathcal{B}} \rangle$. A circle's colour indicates the expected synchronizability $\langle R \rangle$. Squares represent real-world networks reported to display a small-world topology (Supplementary Table 1). We chose ξ_L and ξ_C so that networks of different sizes can be compared w.r.t. average shortest path L and clustering coefficient C, quantities that characterize small-worldness[8]. $(\xi_L, \xi_C) = (0, 0)$ labels a regular network whereas $(\xi_L, \xi_C) = (1, 1)$ labels a random network. Small-world networks reside in the top left quadrant. See next section for details on the ξ_X, $X = L$ or C.

2.2.4 Small-World Networks with Different Link Length Distributions

Here we study small-world networks with different link length distributions. The networks are created as follows: We start with a 2-dimensional lattice in which every node is connected to its 4 nearest neighbours. Then we add short-cuts so that, in the end, the average number of links per node is 8. For short-cut addition, we use the following procedure[30]: A pair of nodes, (i, j) is chosen randomly. Then a new link connecting them is added to the network with probability

$$P(r) \propto r^{-\alpha},$$

where r is the Manhattan distance between i and j, i.e., the distance between them on the original 2-dimensional lattice with no short-cuts.

In networks created like this, we expect the length of a typical short-cut to decline when α increases. How do basin stability and synchronizability depend on α?

To investigate this, we choose the network size to be $N = 20 \cdot 20 = 400$ and, as before, place a Rössler oscillator at each node. Then for every network, we compute $\bar{S}_{\mathcal{B}}$. Here, we use a slightly smaller reference subset, $\mathcal{Q} = q^N$ with $q = [-15, 15] \times [-15, 15] \times [-3, 35]$, than above as otherwise the values of $S_{\mathcal{B}}$ are too small to be accuractely measurable with $T = 500$ integrations (cf. Methods). Note that the Rössler attractor is still included in q. Finally, we average $\bar{S}_{\mathcal{B}}$ over the ensemble to obtain $\langle \bar{S}_{\mathcal{B}} \rangle$.

Supplementary Fig. S10a shows that expected synchronizability $\langle R \rangle$ declines as α increases. This means that, from the linear stability perspective, an optimal link length distribution should fall off slowly or not at all (corresponding to rather low α).

The perspective of basin stability, again, disagrees with this. In Supplementary Fig. S10b, we see that $\langle \bar{S}_{\mathcal{B}} \rangle$ evolves in an opposite way to expected synchronizability in a large portion of the parameter interval: $\langle \bar{S}_{\mathcal{B}} \rangle$ grows as α increases. Finally, as α is tuned up further, basin stability reaches a maximum and then declines rapidly towards zero as synchronizability

approaches the stability threshold.

We think that these results do not contain considerably more information than Fig. 3 and Supplementary Fig. S8: For large α as well as for small p, networks have an intense local structure that is reduced as α decreases and p increases. This may be the common reason behind the phenomena we observe.

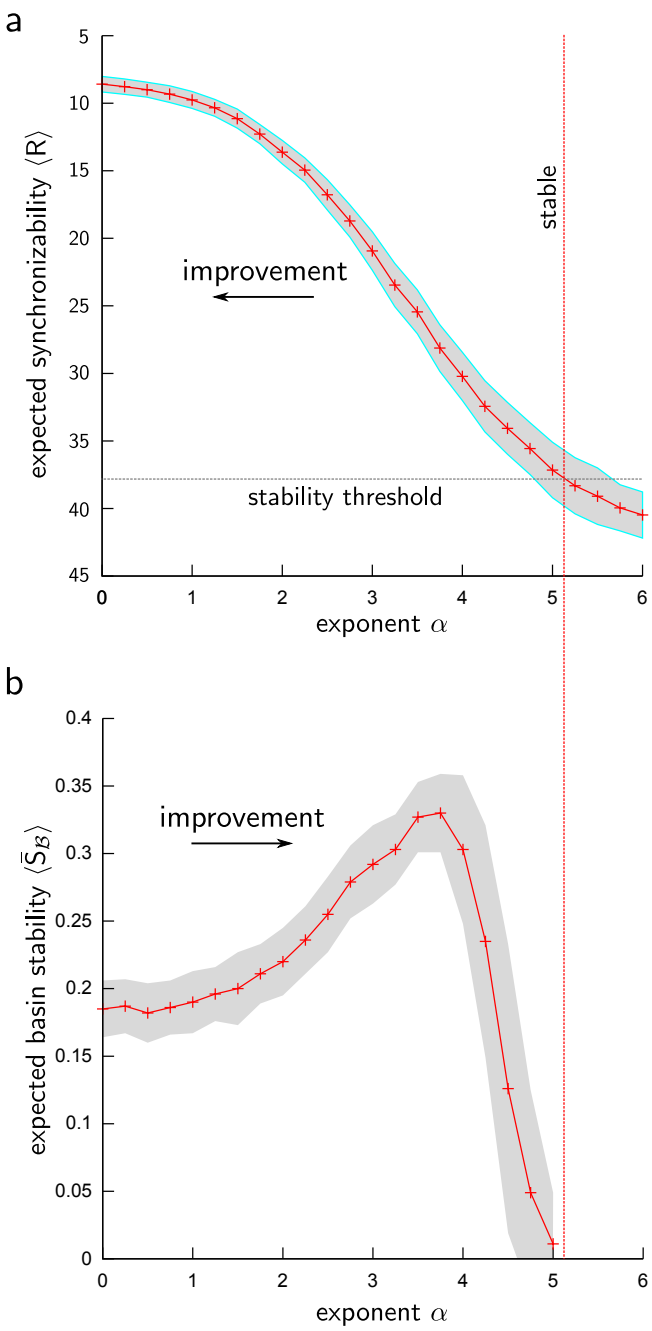

Figure S10: **Synchronizability and basin stability in networks of chaotic oscillators with different link length distribution. a**: Expected synchronizability $\langle R \rangle$ versus the link length distributions's parameter α. The scale of the y-axis was reversed. The grey shade indicates $\pm$ one standard deviation. **b**: Expected basin stability $\langle \bar{S}_{\mathcal{B}} \rangle$ versus α. The grey shade indicates $\pm$ one standard deviation. Solid lines are guides to the eye. The plots shown were obtained for $N = 400$ oscillators of Rössler type, each having on average $k = 8$ neighbours.

2.3 Properties of Studied Real-World Networks

Many synchronizing real-world networks were reported to display a small-world topology, among them neural networks and power grids[8,9]. We supply an overview of typical network properties for some such networks in Supplementary Table S1. Therein, L measures the average shortest path length between two vertices in the network and $C = \frac{1}{N}\sum C_i$ is the average of the nodal clustering coefficients

$$C_i = \frac{\sum_{j,k\in \mathsf{N}(i)} A_{jk}}{|\mathsf{N}(i)|^2 - |\mathsf{N}(i)|}.$$

In this formula, A is the adjacency matrix, $\mathsf{N}(i)$ is the set of nodes to which node i is linked, and $|\mathrm{N}(i)| = \sum_{j\in \mathsf{N}(i)} 1$ its cardinality[35].

A network is said to display a small-world topology if $C \gg C_{\mathrm{R}}$ and $L \approx L_{\mathrm{R}}$, where C_{R} and L_{R} are the average values of C and L in a random network that has the same number N of nodes and the same number E of edges[8]. To estimate C_{R} and L_{R}, we apply the Watts-Strogatz (WS) algorithm with rewiring probability $p = 1$ to regular ring lattices of given N and E and average over many realizations. The initial regular ring lattices are created in two steps. First, connect every node to its k nearest neighbours, where k is the largest even integer smaller than $\beta E/N$ with $\beta = 2$ ($\beta = 1$) for undirected (directed) networks. Second, add the remaining $E - kN/\beta$ edges randomly between nodes that are $k/2+1$ steps apart on the ring[9]. In Supplementary Table S1, beside C_{R} and L_{R} we report the averages C_{L} and L_{L} for lattice-like networks.

From the WS model's perspective, C and L assume their largest values in regular lattices and their lowest values in random graphs. Hence, small-world networks are rather similar to regular lattices w.r.t. C, yet at the same time rather similar to random graphs w.r.t. L. To quantify these similarities independently of the network size (as given by

N, E), we introduce

$$\xi_X = -\frac{\log(X/X_{\mathrm{L}})}{\log(X_{\mathrm{L}}/X_{\mathrm{R}})} = 1 - \frac{\log(X/X_{\mathrm{R}})}{\log(X_{\mathrm{L}}/X_{\mathrm{R}})}$$

with $X = L$ or C. ξ_X counts how many of orders of magnitude X is away from X_{L} in relation to the number of orders of magnitude between X_{L} and X_{R}. Note that $\log C$ can be interpreted as a measure of dimensionality[36]. Lattices have $\xi_C = \xi_L = 0$, whereas random graphs have $\xi_L = \xi_C = 1$. From the above, small-world networks should display ξ_C not too far from 0 and ξ_L not too far from 1 (and indeed the real networks studied here do so, see Fig. 4). We use ξ_C and ξ_L to topologically compare the networks listed in Supplementary Table S1 to the ensemble results on basin stability and synchronizability reported in the main text.

#	Network	N	E	C	L	C_{R}	L_{R}	C_{L}	L_{L}
1	Macaque Visual Cortex	30	311	0.53	1.73	0.36	1.66	0.66	1.93
2	Macaque Cortex	71	746	0.46	2.38	0.15	2.03	0.66	3.85
3	Cat Cortex	52	820	0.55	1.81	0.31	1.70	0.69	2.14
4	C. Elegans Neural Network	297	2345	0.18	3.99	0.027	2.98	0.64	19.25
5	Power Grid of Western US	4941	6594	0.08	18.99	0.00035	10.19	0.39	925.7
6	Power Grid of Central Europe	4335	5551	0.07	28.73	0.00020	10.73	0.35	846.8
7	Power Grid of Northern Europe	524	640	0.04	14.49	0.0030	8.38	0.29	107.6
8	Power Grid of the UK	393	484	0.04	12.54	0.0034	7.78	0.30	80.3

Supplementary Table S1: **Overview of properties of some real-world networks.** N specifies the number of nodes and E the number of edges in the network. Furthermore, L is the average shortest path length and C the clustering coefficient. These two quantities have been widely used to characterize small-worldness[8]. X_{R} (or X_{L}) represent average values of X computed in random networks (or lattices) of the same N, E, where $X = L, C$. For networks 1 to 3, the values of L and C were taken from ref. 9.

2.4 Non-Convexity of the Basin in Rössler-networks

Convexity of the basin $\mathcal{B}$ of the synchronous state in a network of Rössler oscillators would make the computation of its volume simpler. However, we clearly find that $\mathcal{B}$ is not convex. This follows from the non-convexity of the chaotic attractor's basin $\mathcal{B}_1$ of a single Rössler oscillator, as obvious from the two-dimensional details displayed in Supplementary Fig. S11. $\mathcal{B}_1^N := \{\mathbf{r}_1 = \ldots = \mathbf{r}_N = \mathbf{r} \mid \mathbf{r} \in \mathcal{B}_1\}$ is a subset of the synchronous state's basin $\mathcal{B}_N$ for every $N \geq 1$. Consequently, $\mathcal{B}_N$ is not convex either. Hence the powerful tools for volume estimation of convex bodies are not applicable here.

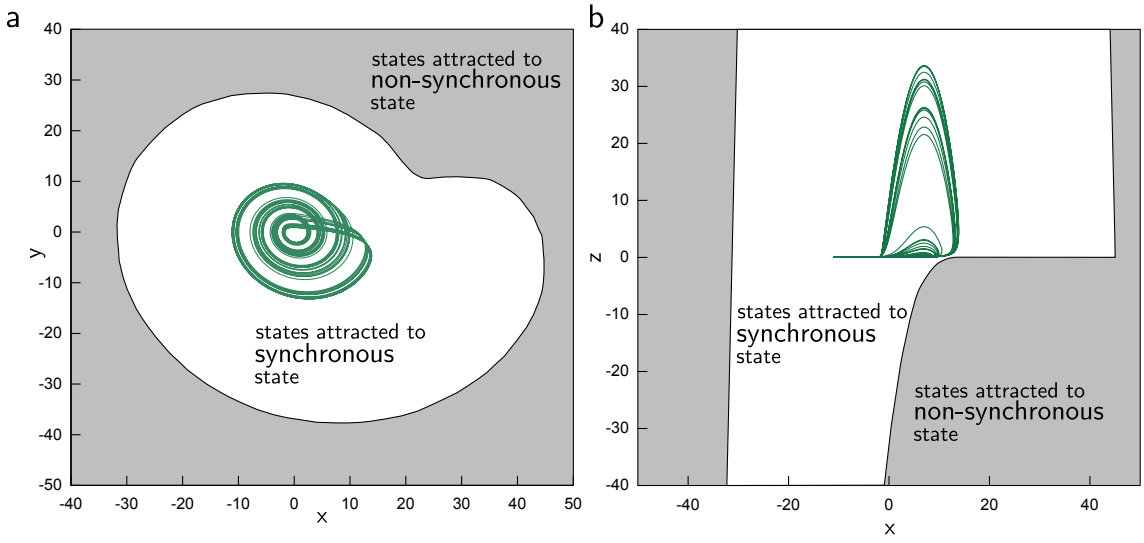

Supplementary Figure S11: **Two-dimensional details of the Rössler attractor's basin**. **a:** shows the xy-detail. A point (x, y) refers to the initial state $(x, y, 0)$. **b:** shows the xz-detail. A point (x, z) refers to the initial state $(x, 0, z)$. In both panels the white region indicates the Rössler attractor's basin of attraction. The green shape depicts a two-dimensional projection of the Rössler attractor.

References

[31] Levins, R. Some demographic and genetic consequences of environmental heterogeneity for biological control. *Bull. Entomol. Soc. Am.* **15**, 237–240 (1969).

[32] Tilman, D. Competition and biodiversity in spatially structured habitats. *Ecology* **75**, 2–16 (1994).

[33] Kuehn, C. A mathematical framework for critical transitions: Bifurcations, fastslow systems and stochastic dynamics. *Physica D* **240**, 1020 – 1035 (2011).

[34] Dakos, V., Scheffer, M., van Nes, E.H., Brovkin, V., Petoukhov, V. & Held, H. Slowing down as an early warning signal for abrupt climate change. *Proc. Natl. Acad. Sci. USA* **105**, 14308–14312 (2008).

[35] Newman, M.E.J. The structure and function of complex networks. *SIAM Rev.* **45**, 167–256 (2003).

[36] Donner, R.V., Heitzig, J., Donges, J.F., Zou, Y., Marwan, N. & Kurths, J. The geometry of chaotic dynamics – a complex network perspective. *Eur. Phys. J. B* **85**, 653 – 672 (2011).